Appl. Phys. B 65, 93–99 (1997)

Applied Physics B Lasers and Optics

Infrared degenerate four-wave mixing and resonance-enhanced stimulated Raman scattering in molecular gases and free jets

D. Voelkel[1], **Yu.L. Chuzavkov**[2], **J. Marquez**[1], **S.N. Orlov**[2], **Yu.N. Polivanov**[2], **V.V. Smirnov**[2], **F. Huisken**[1]

[1] Max-Planck-Institut für Strömungsforschung, Bunsenstr. 10, D-37073 Göttingen, Germany
(Fax: +49-551/5176-704, E-Mail: fhuiske@gwdg.de)
[2] General Physics Institute, Russian Academy of Sciences, Vavilov Str. 38, 117942 Moscow, Russia

Received: 1 October 1996/Revised version: 6 January 1997

Abstract. Infrared degenerate four-wave mixing spectroscopy (IR-DFWM) has been employed to study the molecules acetylene (C_2H_2), methane (CH_4), carbon dioxide (CO_2), and nitrous oxide (N_2O) in a cell under equilibrium conditions and cooled in free jet expansions. For methane at room temperature the detection limit was 2×10^{12} molecules per cm^3 and quantum state, enabling the detection of trace species with a spatial resolution of $1\,mm^2 \times 30\,mm$. In an attempt to study transitions in the $\nu_1 + \nu_3$ and $2\nu_2 + \nu_3$ combination bands of CO_2 or N_2O, it was not possible to observe any DFWM signal. Instead a surprisingly strong, backward- and forward-directed emission was found which could not be attributed to the DFWM process. The signal arising from this emission was more than 2 orders of magnitude stronger than the DFWM signals obtained for other molecules. The frequencies of the emitted radiation were found to correlate with the transitions $\nu_1 + \nu_3 \rightarrow \nu_1$ and $2\nu_2 + \nu_3 \rightarrow 2\nu_2$, respectively. Our investigations lead to the conclusion that the emission can be explained by stimulated Raman scattering, resonantly enhanced by transitions to the combination levels $\nu_1 + \nu_3$ and $2\nu_2 + \nu_3$. This process seems to suppress the generation of DFWM signals.

PACS: 42.65.-k; 33.20.Ea; 47.40.Ki

Resonant degenerate four-wave mixing (DFWM) as a spectroscopic method combines the advantage of high spatial and temporal resolution with low detection limits [1, 2]. During the last few years, this technique has been employed in different wavelength regions for various applications [3–5]. An overview may be found in the review article by Hall and Whitaker [6]. DFWM in the near and middle infrared (IR-DFWM) is of special interest since many molecules have rotational-vibrational transitions in this region [7–11]. In addition, the transitions take place in the electronic ground state, which is important if electronically excited states are not accessible with standard laser systems.

IR-DFWM has been demonstrated to be a valuable tool for the detection of a number of small polyatomic molecules such as HF [7], HCl [8], NO_2 [8], CH_4 [9, 10], and C_2H_2 [9, 10]. So far, the lowest detection limit of 10^{10} molecules per cm^3 was reported by Van der Wal et al. [7] for HF. First IR-DFWM experiments in supersonic jets of acetylene were carried out by Tang and Reid [12]. The IR-DFWM technique is considered to be rather universal [10] and up to now no principle limitations have been reported as far as its applicability as a spectroscopic tool for the detection of molecules in the IR is concerned.

The aim of our study was to explore the applicability of IR-DFWM to the investigation of small polyatomic molecules in supersonic jets with the future intention of extending the technique to the study of molecular clusters. The first experiments were carried out for methane (CH_4) under static conditions to obtain information on the sensitivity and detection limit. Then the technique was applied to C_2H_2 and CH_4 molecules in freely expanded supersonic jets. In this paper we present typical spectra obtained so far and give an estimation for the cooling achieved in the jet.

When we studied CO_2 and N_2O, exciting transitions in the $\nu_1 + \nu_3$ and the $2\nu_2 + \nu_3$ combination bands, we were not able to observe any DFWM signal either in the static gas cell or in the supersonic jet. Instead, we detected a rather strong infrared radiation emitted in both forward and backward directions of each incident beam. Only one incident beam was required to generate this stimulated emission. The effect was only observed if the laser pulse energy exceeded a (rather low) threshold which was a function of the gas pressure. We have investigated the generation of this stimulated emission under various conditions and present the results which show that the emission can be explained by resonance-enhanced stimulated Raman scattering.

1 Experimental setup

A schematic view of the experimental setup is shown in Fig. 1. The experiment employs an injection-seeded single-longitudinal-mode Nd:YAG laser (Continuum NY 81-20 C) operated at a repetition rate of 10 Hz. An intracavity aperture ensures a Gaussian beam shape. The main part (90%) of the energy of the frequency-doubled radiation at 532 nm is used

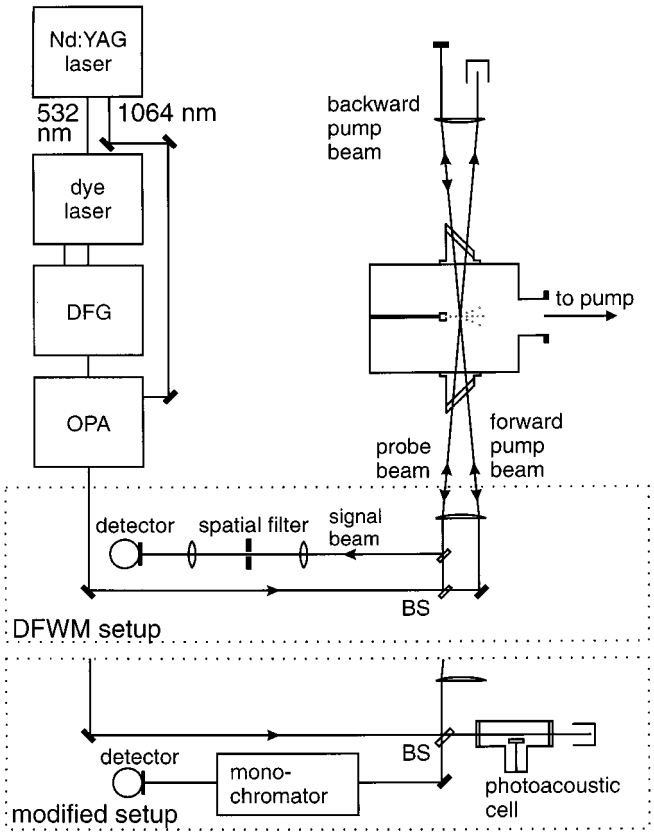

Fig. 1. Schematic view of the experimental setup. The upper part depicts the setup used for DFWM experiments. The modified setup displayed in the bottom of the figure is used to study the stimulated emission observed in the experiments with CO_2 and N_2O

to pump a tunable dye laser (Lambda Physik, Scanmate 1E) operated with DCM dye. The dye-laser beam has a spectral bandwidth of $0.12\,cm^{-1}$. For the DFWM experiment carried out in a supersonic jet of methane, an intracavity etalon was employed to reduce the bandwidth to $0.03\,cm^{-1}$. In a difference-frequency generation stage (DFG), the output of the dye laser is mixed with the residual 10% of the 532 nm beam to produce IR radiation in the frequency range between 2700 and $3900\,cm^{-1}$ [13]. A $LiIO_3$ crystal provides the nonlinear medium for the difference-frequency generation. The IR pulses generated by DFG have an energy of approximately $10\,\mu J$ and serve as seeder at the idler frequency for an optical parametric amplifier (OPA). The OPA consists of two $LiNbO_3$ crystals pumped by the fundamental of the Nd:YAG laser. With a pump energy of 130 mJ/pulse, we achieved an idler pulse energy of more than 2 mJ, with an estimated pulse duration of about 5 ns. The idler radiation of the OPA is separated from the pump and signal waves by four dichroic mirrors. After these mirrors, a copropagating HeNe laser is used for visual alignment of the infrared beam. The bandwidth of the generated IR beam is determined by the convolution of the bandwidths of the dye laser, the 532 nm, and the 1064 nm radiation. Since the injection-seeded Nd:YAG laser has a bandwidth of $0.004\,cm^{-1}$, which is almost an order of magnitude smaller than the smallest dye laser bandwidth, the width of the tunable IR radiation is practically determined by the dye laser. For simplicity, the idler radiation is referred to as laser radiation, although it is generated in a nonlinear optical mixing process.

In the DFWM experiment, a standard phase-conjugate geometry is employed in which a 50% beam splitter (BS) splits the laser beam into a probe and a forward pump-beam. A retro-reflecting gold mirror, positioned behind the probe region, produces the backward pump-beam. Two focusing CaF_2 lenses ($f = 300$ mm) are placed symmetrically around the interaction region. In an alternative geometry, these lenses are replaced by a single focusing lens ($f = 1000$ mm), placed in front of the first beam splitter. With this variant a less tight focusing is achieved. Another 50% beam splitter in the probe-beam path extracts the phase-conjugate signal. After a beam path of 2.5 m the signal is spatially filtered and focused onto an InSb detector with an active-area diameter of $250\,\mu m$.

In order to investigate the stimulated emission observed in the experiments with CO_2 and N_2O in more detail, some changes are made, which are shown as "modified setup" in the lower part of Fig. 1. In this configuration a single IR beam is reflected by a 50% beam splitter into the main gas cell. The transmitted beam enters a separate cell to perform photoacoustic absorption spectroscopy. The backward–directed stimulated emission, created in the main gas cell, passes through the beam splitter and is dispersed in a monochromator (Mc Pherson model EUE-700), containing a grating with 150 lines/mm. Finally the transmitted radiation is detected by one of the following three detectors: (a) a liquid-nitrogen-cooled InSb detector, (b) a pyroelectric detector, and (c) a liquid-nitrogen-cooled Ge:Au detector.

The probe volume is placed in a 45 cm × 20 cm × 15 cm stainless–steel vessel which serves as static gas cell or as molecular beam source chamber. For the latter purpose it contains a fuel-injection-type pulsed nozzle, which can be translated in three directions relative to the focus of the laser beams. The optical path length between the two CaF_2 windows, mounted at the Brewster angle, is 22 cm. For the jet experiments either a thin-walled orifice nozzle with a diameter of 1 mm or a conical nozzle is used. The latter has an inner diameter of 0.6 mm, a length of 1.8 mm, and an opening angle of 30°. A mechanical pump ($65\,m^3/h$) and a roots blower ($350\,m^3/h$) supply sufficient pump capacity. Pressures are measured by a capacitance manometer (Baratron) and a thermocouple gauge tube.

During each dye-laser scan, all crystals are angle-tuned under control of a personal computer to ensure optimum phase-matching. The transient signals are preamplified and averaged in a digital sampling oscilloscope (Tektronix, model TDS 350). Finally the waveform is transferred to the computer and integrated numerically.

2 Results and discussion

2.1 Degenerate four-wave mixing

In the first part of this chapter, we will discuss the detection limit achieved with the DFWM setup just described. In addition, we will present DFWM spectra of CH_4 and C_2H_2 recorded in free jet expansions and discuss the manifestation of rotational cooling in the jet.

The first DFWM experiment was performed on CH_4 under static conditions using a laser energy of about 750 μJ/pulse and a bandwidth of 0.12 cm^{-1}. The spectra were recorded in the alternative DFWM geometry with a single focusing lens ($f = 1000$ mm). The R(0) line in the ν_3 band of CH_4 at room temperature was used to determine the detection limit. At a partial pressure of 0.06 mbar CH_4 diluted in nitrogen at a total pressure of 5 mbar, we determined a signal-to-noise ratio of 45. Assuming a quadratic dependency of the signal on the number density, this leads to a detection limit of 0.009 mbar (equivalent to 2.4×10^{14} molecules per cm^3).

Methane exists in three practically non-interacting nuclear spin modifications A, E, and F, which occur at room temperature with the abundance ratio 5 : 2 : 9 [14]. For $J = 0$, CH_4 only exists in the A modification. The probability of finding a molecule of this modification at room temperature in $J = 0$ is, applying Eq.(4) in [15], $P_{T=A}(J = 0) = 5/16 \times 5/185.4 = 0.0084$. With these numbers taken into account, the detection limit is determined to be 2×10^{12} molecules per cm^3 and quantum state.

DFWM spectra of the Q-branch of the ν_3 vibration of CH_4 measured in the expansion of a pulsed supersonic jet of neat methane (Praxair, purity 99.995%) are shown in Fig. 2. Employing the 1 mm diameter pinhole nozzle, the stagnation pressure was held constant at 650 mbar. The distance between probing volume and nozzle exit was varied from $x = 4$ mm (upper spectrum) to 19 mm (lowest spectrum). The laser beams were focused by a 1000 mm focusing lens. In this experiment, the intracavity etalon of the dye laser has been used to reduce its bandwidth to 0.03 cm^{-1}. The frequency was scanned in steps of 0.01 cm^{-1} and the DFWM signal was averaged over 30 laser pulses. The laser energy per pulse was 80 μJ. The various transitions, as indicated in the top of the figure, are assigned according to Pine [16].

The peaks corresponding to low rotational states gain in intensity at the expense of the higher-level lines when the distance between the interaction region and the nozzle is increased. Each modification is cooled separately, because the probability for interconversion is extremely small. Most lines observed belong to the F modification. At a small distance from the nozzle exit ($x = 4$ mm), population in rotational levels up to $J = 4$ is observed. In contrast, at $x = 19$ mm only the rotational states $J = 1$ and $J = 2$ appear, which are the two lowest levels of this modification. For the A modification, only the levels $J = 0$, 3, 4, 6, 7, etc. can be populated in the vibrational ground state. Since a Q-branch transition does not exist for $J = 0$ [14], the $J = 3$ level is the lowest rotational state which can be observed. The corresponding two lines are present in the two upper spectra. Due to the rotational cooling, the population is transferred to $J = 0$ at larger distances from the nozzle, which cannot be probed by a Q-branch transition. The rotational ground state for the E modification is $J = 2$. This level is observed in all three spectra, while the higher rotational states $J = 4$ and $J = 5$ are only populated close to the nozzle.

Figure 3 shows a C_2H_2 spectrum recorded in the pulsed expansion of neat C_2H_2 (Messer Griesheim, purity 99.6%) through the conical nozzle at a backing pressure of 1 bar. The nozzle exit was placed at a distance of 10 mm from the interacting laser beams, which were focused by the lenses with 300 mm focal length. Each data point was averaged over 32 laser pulses, and the separation between the points was chosen to be 0.0125 cm^{-1}, which corresponds to 1/10 of the laser bandwidth. The spectrum was recorded at a laser energy of 80 μJ/pulse. The linewidth of the observed transitions is the same as the laser bandwidth.

The observed lines correspond to transitions from the ground state to the ν_3 and $\nu_2 + \nu_4 + \nu_5$ vibrational states as indicated below the spectrum. For the R branch of the $\nu_2 +$

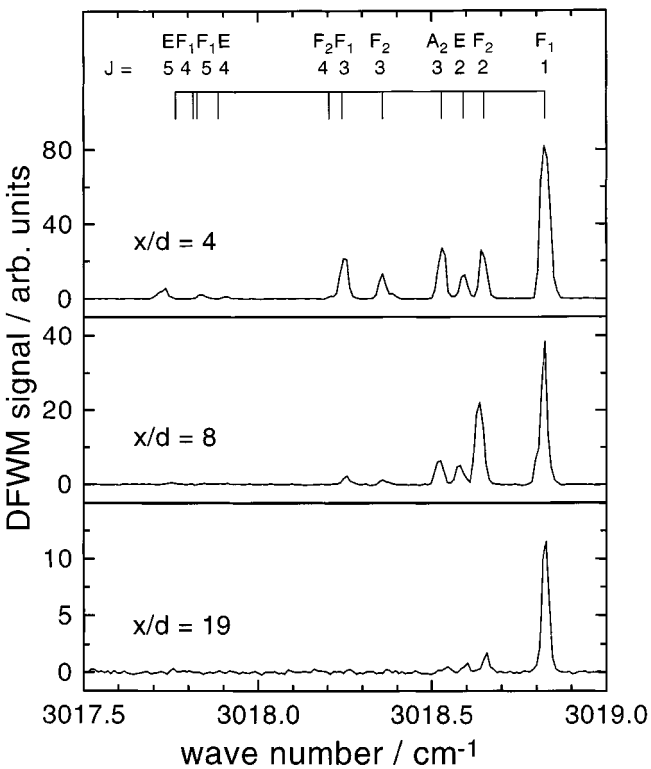

Fig. 2. IR-DFWM spectra of jet-cooled methane in the ν_3 Q branch as a function of the distance between probe volume and nozzle exit. The backing pressure was kept constant at 650 mbar. The laser bandwidth was 0.03 cm^{-1}. Line positions and assignments are indicated in the top of the figure

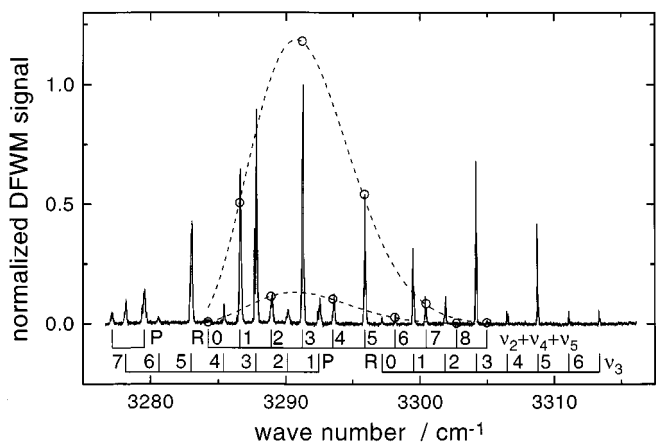

Fig. 3. IR-DFWM spectrum of jet-cooled acetylene in the region of the $\nu_3/\nu_2 + \nu_4 + \nu_5$ Fermi dyad. The line positions are indicated in the bottom of the figure. The dashed curves and open circles represent the IR-DFWM intensity distributions for the two nuclear spin modifications of acetylene as calculated for a temperature of 35 K. The laser bandwidth was 0.12 cm^{-1}

$\nu_4 + \nu_5$ vibrational band, which was recorded up to $J = 10$, we calculated the DFWM intensity distributions as indicated in the figure by the open circles and dashed curves. Acetylene belongs to the point group $D_{\infty h}$; therefore odd and even rotational levels have different statistical weights. Just as for H_2, the odd levels are three times more populated than the even levels. Since the DFWM line intensities are proportional to the square of the population, the odd rotational lines are 9 times stronger. The intensities were calculated as described by Williams et al. [17]. Best agreement with the measured data was achieved for a rotational temperature of 35 K. A more detailed discussion of the rotational temperature analysis can be found in the paper of Tang and Reid [12] who investigated supersonic jets of C_2H_2 in the same spectral region.

The experiments just described show that IR-DFWM spectra of CH_4 and C_2H_2 in supersonic jet expansions were realized with a signal to noise ratio of more than 100 on the strongest lines.

2.2 Resonance-enhanced stimulated Raman scattering

When we tried to study CO_2 and N_2O with our DFWM setup, we were not able to detect the DFWM signal either under static conditions in the cell or in the jet. Instead, we observed a rather strong stimulated emission which we interpret as resonance-enhanced stimulated Raman scattering. In this section, we will discuss the experiments which led us to this conclusion.

For simplicity, we will use the notation of Herzberg [14] to denote the vibrational levels of CO_2 and N_2O. According to newer measurements performed by Rothman and Young [18], the origin of the $\nu_1 + \nu_3$ band of CO_2 is at $3714.78\,\mathrm{cm}^{-1}$. These authors use the AFGL notation in which the $\nu_1 + \nu_3$ vibration corresponds to the 10 011 state. The $2\nu_2 + \nu_3$ combination vibration, with the origin at $3612.84\,\mathrm{cm}^{-1}$, corresponds to the 10 012 state in the AFGL notation.

Investigating CO_2 (Praxair, 99.998% purity) and N_2O (Praxair, 99.998% purity) under static conditions in the pressure range between 0.01 mbar and 1 bar with various laser energies (up to 2 mJ/pulse), no DFWM signal could be detected, although the laser frequency was tuned to be in resonance with various transitions in the $\nu_3 + \nu_1$ and $2\nu_2 + \nu_3$ combination bands for both molecules. Instead, we observed a different signal with a rather high intensity, whenever the laser frequency was in resonance with an absorption line. This signal was also present when the forward pump beam (see Fig. 1) was blocked; i.e. it was not created by DFWM. The focused probe-beam alone was sufficient to generate this radiation. More careful inspection revealed that an infrared beam was emitted in both forward and backward directions whenever the laser intensity exceeded a threshold, which was a function of the gas pressure. At a CO_2 pressure of 50 mbar, the emission occurred already at laser energies of 10 μJ per pulse, while for a pressure of 1 mbar the threshold was found to be 50 μJ/pulse. The 300 mm focusing lenses were used in these experiments.

Whenever the stimulated emission was first observed, its intensity was high enough to saturate the InSb detector. Measurements with a power meter revealed that the energy ratio of the backward stimulated emission to the pump energy was 0.8% at a laser energy of 2 mJ/pulse and a laser bandwidth of $0.12\,\mathrm{cm}^{-1}$. For this measurement the laser was in resonance with the P(3) line of the $2\nu_2 + \nu_3$ transition in CO_2. The CO_2 pressure was 50 mbar.

For N_2O we also observed stimulated emission whenever the laser was in resonance with transitions to the $\nu_1 + \nu_3$ and $2\nu_2 + \nu_3$ combination levels, but the threshold for the laser power was approximately one order of magnitude higher. The emission showed the same characteristics, and therefore we will concentrate on the experiments with CO_2 and only note the differences observed for N_2O.

This type of stimulated emission was first observed by Finizi and Moore [19] in their laser-induced fluorescence experiments when they excited strong vibrational-rotational transitions in the $\nu_1 + \nu_3$ combination band of CO_2. However, they did not investigate the origin of this radiation in detail.

To investigate the emission, we modified our setup to create and collect the backward–directed stimulated emission more efficiently (see Fig. 1). We concentrated our studies on the backward–directed stimulated beam, because this beam could easily be separated from the incident laser beam. In addition, a less sensitive Au:Ge detector with a larger dynamic range was employed to detect the signal.

First, the spectrum of the backward–directed emission was analyzed with an IR monochromator. Its maximum resolution was approximately $0.5\,\mathrm{cm}^{-1}$ and the observable wavelength range was between 1.6 and 8 μm. The observed emission spectrum for a fixed incident pump frequency contained only a single line. Exciting the $\nu_1 + \nu_3$ combination band, we found the emission frequency to be close to $2326.6\,\mathrm{cm}^{-1}$, which corresponds to the transition $\nu_1 + \nu_3 \rightarrow \nu_1$. Similarly, exciting the $2\nu_2 + \nu_3$ combination band, the emission frequency was close to $2327.4\,\mathrm{cm}^{-1}$ corresponding to the transition $2\nu_2 + \nu_3 \rightarrow 2\nu_2$. When we tuned the frequency of the incident IR radiation to other rotational lines within the same bands, the frequency of the stimulated emission shifted accordingly. If P-branch transitions were excited the frequency of the stimulated emission shifted to smaller values with increasing J'' while for R-branch transitions the opposite behavior was observed.

To illustrate the transition scheme, part of the CO_2 energy level diagram is shown in Fig. 4. As an example, we will discuss the transitions to the combination band $\nu_1 + \nu_3$. The rotational selection rules are $\Delta J = \pm 1$, i.e. we have R and P branches. Due to the symmetry of the CO_2 molecule, only even rotational levels exist in the vibrational ground state. The allowed transitions are indicated by upward–directed arrows. The selection rules for the emission $\nu_1 + \nu_3 \rightarrow \nu_1$ are again $\Delta J = \pm 1$. Thus, starting from any excited rotational level, two different transitions are allowed, as indicated by the downward–directed arrows.

We always observed only one emission line with a signal-to-noise ratio of 100 or larger for one particular excitation. Since the separation of the two allowed emission lines from one level is at least $2\,\mathrm{cm}^{-1}$[e.g. $E(\nu_1, J''' = 2) - E(\nu_1, J''' = 0) = 2.34\,\mathrm{cm}^{-1}$] and the resolution of the monochromator is $0.5\,\mathrm{cm}^{-1}$, we would have been able to resolve this separation. Thus it appears that the transition corresponding to one specific ΔJ is much stronger than the other one. We found this to be the transition where $\Delta J = J''' - J'' = 0$ for the rotational levels of the ground and final state. In other words, after a P (or R) excitation, the emission occurs only as a P

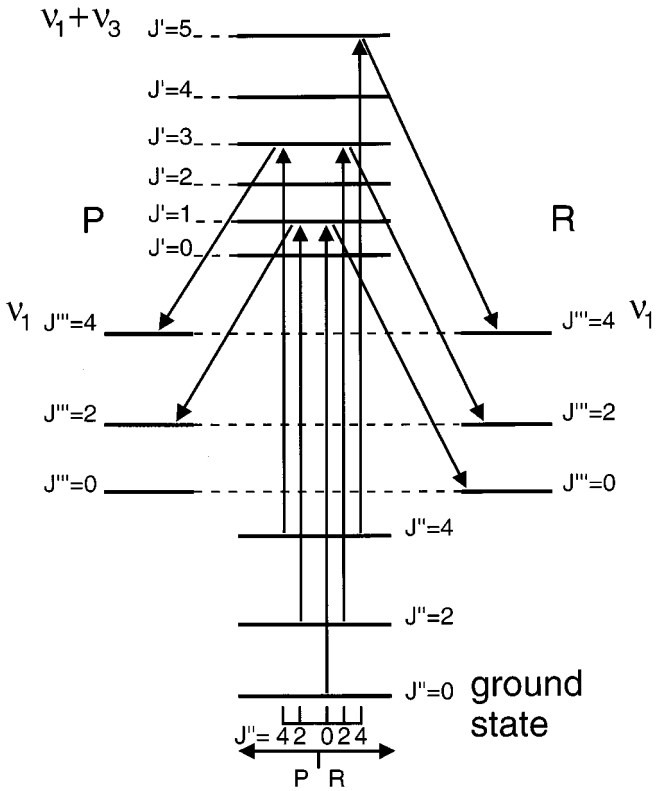

Fig. 4. Schematic energy level diagram of CO_2 showing the ground and vibrationally excited states

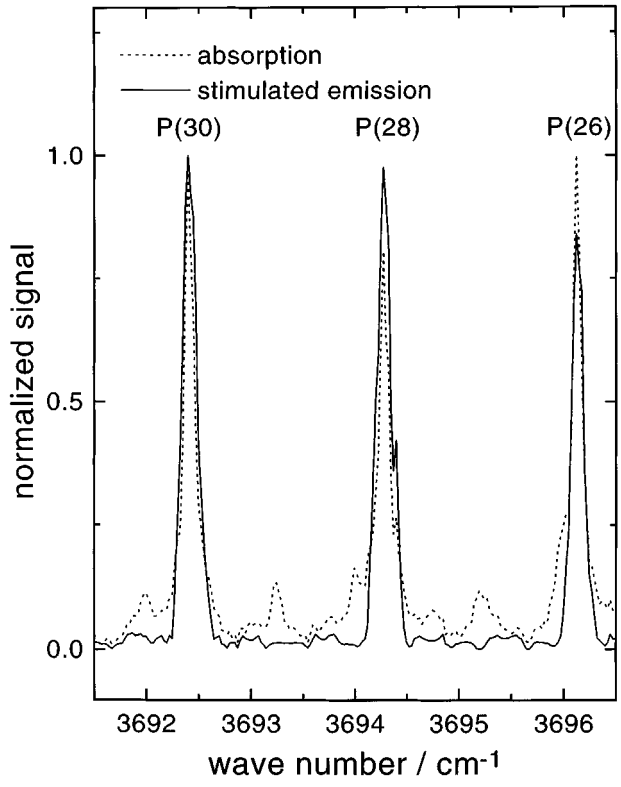

Fig. 5. Simultaneously recorded excitation (*solid line*) and photoacoustic (*dashed line*) spectra of CO_2 covering three lines in the P branch of the $\nu_1 + \nu_3$ combination band. The pressure in both gas cells was 20 mbar

(or R) transition. The excitation with the following emission can be considered as a Q-branch Raman transition, which is known to be rather strong. The other allowed emission line would correspond to a much weaker O- or S-branch Raman transition. This offers an explanation why only one line is observed.

In the next experiment, the total intensity of the backward–directed stimulated emission was recorded while the incident IR radiation was tuned over several transitions from the ground state to the $\nu_1 + \nu_3$ and $2\nu_2 + \nu_3$ combination vibrations. To distinguish these spectra from the emission spectra discussed before, they are called excitation spectra. The monochromator was removed from the beam path. We observed stimulated emission whenever the frequency of the incident radiation was coincident with a P or R transition in either combination band. The transitions were identified by a photoacoustic absorption spectrum of CO_2, simultaneously recorded in a separate cell (see Fig. 1). Typical excitation and absorption spectra, covering three transitions [P(26), P(28), and P(30)] of the $\nu_1 + \nu_3$ combination band, are shown in Fig. 5. Both were recorded at a CO_2 pressure of 20 mbar.

As can be seen in Fig. 5, we did not observe stimulated emission when the laser radiation was coincident with transitions starting from the $\nu_2 = 1$ vibrational level. In contrast, these hot-band transitions are clearly visible in the absorption spectrum. The width of the emission lines depended strongly on the experimental conditions (laser energy and pressure) as will be discussed below; but the lines were always centered at the same frequencies as the absorption lines.

The stimulated IR radiation has a pulse duration of no more than 10 ns, which is the response time of our fastest detection system. The pulses arrive with the same delay (relative to the pump-laser pulse) as the scattered light that we intentionally created in the focal plane. In general, we did not observe any additional delay for the stimulated emission. Only at low CO_2 pressures and laser intensities very close to the threshold, the stimulated emission intensity became very unstable and had a time jitter. Under these conditions a time delay of up to 25 ns was detected, which strongly varied from shot to shot. However, this effect was only present in a very small pressure range and could not be observed for N_2O.

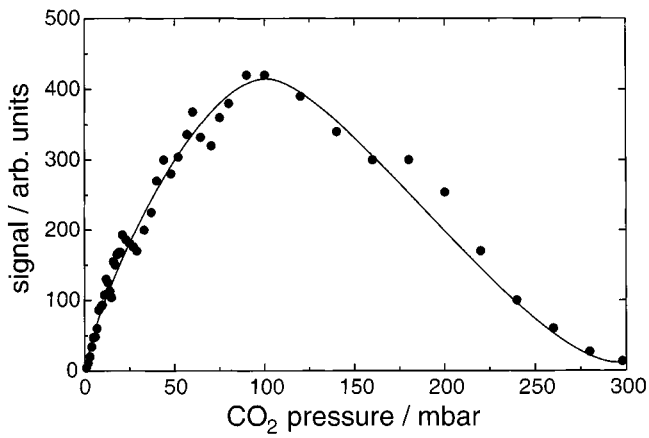

Fig. 6. The backward–directed stimulated emission intensity as a function of the CO_2 pressure. The exciting laser frequency was tuned to the center of the P(28) line in the $\nu_1 + \nu_3$ band

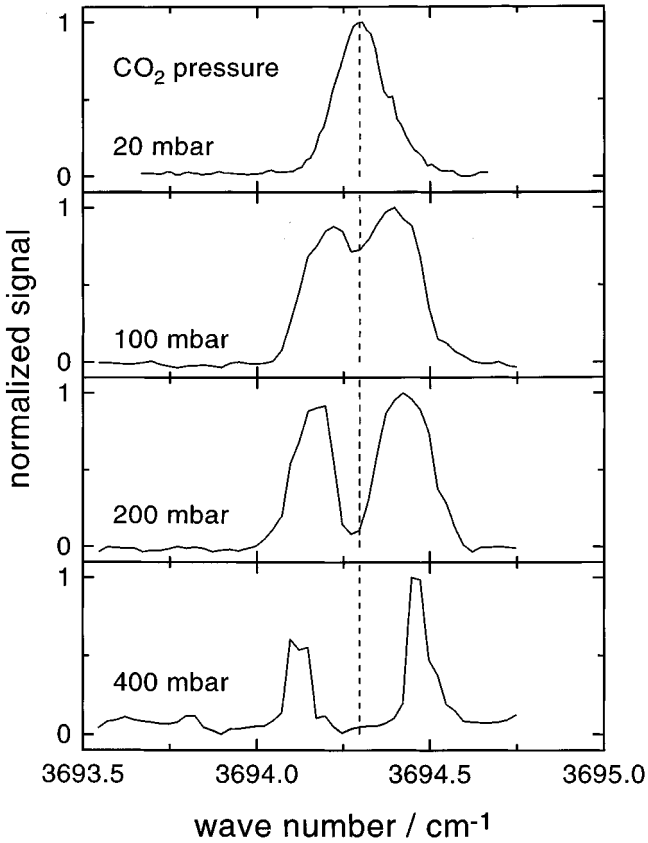

Fig. 7. Development of the excitation spectrum as a function of the CO_2 pressure. The pump laser was scanned over the P(28) line in the $\nu_1 + \nu_3$ band

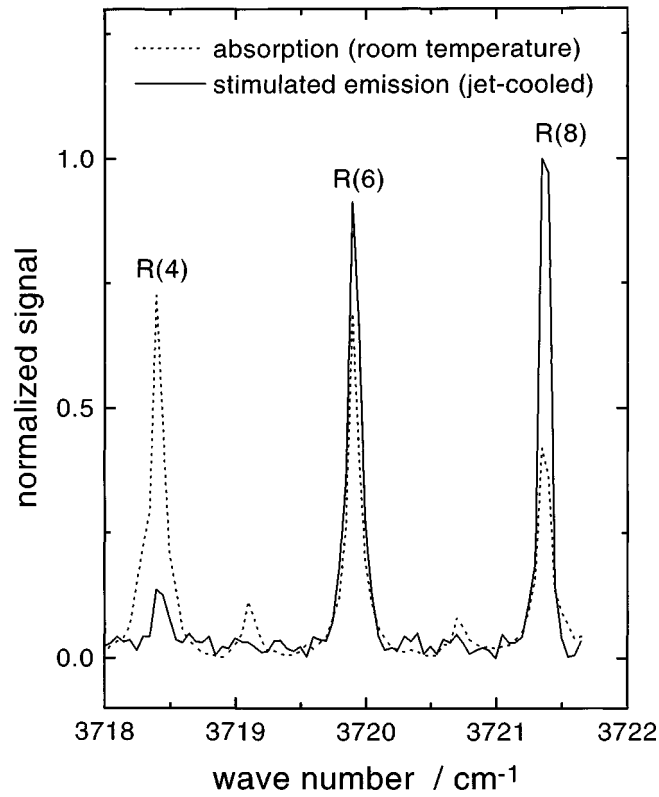

Fig. 8. Excitation spectrum of jet-cooled CO_2 (*solid line*) recorded at a backing pressure of 3 bar and a distance of 3 mm from the nozzle exit. The absorption spectrum (*dashed line*) was simultaneously recorded in a separate static cell filled with 20 mbar CO_2

In the following experiments, we investigated the dependency of the total stimulated emission intensity on the CO_2 pressure, when the incident laser frequency was tuned to the center of the P(28) line in the $\nu_1 + \nu_3$ band. The result is displayed in Fig. 6. Starting from low pressure, the intensity increased and reached a maximum at 100 mbar. At higher pressures the signal decreased, while at pressures above 400 mbar no stimulated emission was observed. The position of the maximum depended on the applied laser energy. A higher pump-energy resulted in a shift of the maximum towards higher pressures. In order to investigate this behavior in more detail, we recorded excitation spectra for different CO_2 pressures at a pump energy of about 1 mJ, while the pump laser was tuned through the same absorption line. These spectra are shown in Fig. 7. At low pressures we found the linewidth to be comparable to the bandwidth of the laser, while an increased pressure led to a broadening of the lines. If the pressure was raised to 100 mbar, where the maximum in Fig. 6 was found, a dip appeared at the center of the line. This dip became more pronounced at higher pressures. At pressures above 500 mbar, the stimulated emission disappeared completely.

A similar behavior was observed earlier in studies of resonant stimulated electronic Raman scattering in atomic systems [20] and in DFWM experiments [21, 22], revealing similar line shapes and pressure dependencies. This was explained by a competition between the nonlinear process and the resonant absorption of the incident laser photons. The stimulated emission intensity, as well as the DFWM intensity, shows a nonlinear dependency on the incident laser power. In both cases the signal is generated in a small region, but linear absorption affects the laser intensity along the entire beam path inside the cell.

Interestingly, it was even possible to observe this stimulated emission under the low-density conditions encountered in a supersonic jet. As an example, a spectrum recorded in the jet is presented in Fig. 8. In this experiment neat CO_2 was expanded through the conical nozzle at a stagnation pressure of 3 bar. The focus of the laser beam was placed 3 mm downstream from the nozzle exit. The laser frequency was tuned through a few R-branch transitions of the $\nu_1 + \nu_3$ combination band. Because of the rotational relaxation in the expansion, it was necessary to excite the CO_2 molecules from their low-lying rotational levels.

Optical pumping of vibrational transitions in molecules is widely used to generate tunable coherent radiation in the medium- and far-infrared wavelength region [23–26]. Therefore, the physical processes (resonant Raman scattering and resonant emission processes) responsible for this stimulated radiation are widely discussed in the literature [23–27].

In particular, Lang et al. [23] obtained the result that the Raman process dominates for all but the lowest pressures. This result is based on experimental studies, but has also been predicted by theoretical considerations. Although the experimental conditions are rather different, we observe a similar behavior in our experiments. For low pressures, close to the threshold, the temporal delay of the stimulated emission rela-

tive to the pump-pulse increases. In this region theoretical calculations predict the onset of non-Raman processes [27].

Comparing our observations with the published results, we come to the conclusion that the stimulated emission in our experiments can be explained by stimulated Raman scattering, resonantly enhanced by transitions to the intermediate states. Further investigations as well as theoretical calculations should be carried out to finally prove the origin of the stimulated emission as stimulated Raman scattering and to understand the interdependency between resonant stimulated Raman scattering and DFWM.

3 Conclusions

We have shown that IR-DFWM is a valuable tool for studying various molecules in the expansion of supersonic jets. This was demonstrated for methane and acetylene. When CO_2 or N_2O gas was exposed to IR laser light resonant with transitions from the ground state to the $\nu_1 + \nu_3$ and $2\nu_2 + \nu_3$ combination levels, a stimulated emission process took place. Our investigations suggest that this emission is primarily caused by resonantly enhanced stimulated Raman scattering. Apparently, IR-DFWM and stimulated Raman scattering are competing processes limiting the applicability of IR-DFWM as a general spectroscopic tool.

Acknowledgements. The authors wish to thank Prof. H. Pauly for his continued interest and support. A grant of the Deutsche Forschungsgemeinschaft (DFG) for the bilateral cooperation between Russia and Germany is gratefully acknowledged. The work at the General Physics Institute has been carried out in the frame of the program *Fundamental Spectroscopy* (project 1577 F).

References

1. P. Ewart, S.V. O'Leary: J. Phys. B **15**, 3669 (1982)
2. P. Ewart, S.V. O'Leary: Opt. Lett. **11**, 279 (1986)
3. P.M. Danehy, R.L. Farrow: Appl. Phys. B **2**, 407 (1996)
4. V. Sick, M.N. Buipham, R.L. Farrow: Opt. Lett. **20**, 2036 (1995)
5. E. Konz, V. Fabelinsky, G. Marowsky, H.-G. Rubahn: Chem. Phys. Lett. **247**, 522 (1995)
6. G. Hall, B.J. Whitaker: J. Chem. Soc. Faraday Trans. **90**, 1 (1994)
7. R.L. Van der Wal, B.E. Holmes, J.B. Jeffries, P.M. Danehy, R.L. Farrow, D.J. Rakestraw: Chem. Phys. Lett **191**, 251 (1992)
8. G.J. Germann, D.J. Rakestraw: Science **264**, 1750 (1994)
9. G.J. Germann, A. Mc Ilroy, T. Dreier, R.L. Farrow, D.J. Rakestraw: Ber. Bunsenges. Phys. Chem. **97**, 1630 (1993)
10. G.J. Germann, R.L. Farrow, D.J. Rakestraw: J. Opt. Soc. Am. B **12**, 25 (1995)
11. A. Dreizler, T. Dreier, J. Wolfrum: Chem. Phys. Lett. **233**, 525 (1995)
12. Y. Tang, S.A. Reid: Chem. Phys. Lett. **248**, 476 (1996)
13. F. Huisken, A. Kulcke, D. Voelkel, C. Laush, J.M. Lisy: Appl. Phys. Lett. **62**, 805 (1993)
14. G. Herzberg: Molecular Spectra and Molecular Structure, New York: Van Nostrand, (1945)
15. F. Huisken, T. Pertsch: Appl. Phys. B **41**, 173 (1986)
16. A.S. Pine: J. Chem. Phys. **97**, 773 (1992)
17. S. Williams, R.N. Zare, L.A. Rahn: J. Chem. Phys. **101**, 1072 (1994)
18. L.S. Rothman, L.D.G. Young: J. Quant. Spectrosc. Radiat. Transfer **25**, 505 (1981)
19. J. Finizi, C.B. Moore: J. Chem. Phys. **63**, 2285 (1975)
20. J.C. White: in *Tunable lasers*, L.M. Mollenauer, J.C. White (eds), Springer-Verlag, 1987, p.115
21. D.M. Bloom, P.F. Liao, N.P. Economou: Opt. Lett. **2**, 58 (1978)
22. J. Gumbel, W. Kiefer: J. Opt. Soc. Am. B **9**, 2206 (1992)
23. P.T. Lang, W. Schatz, T. Kass, A.D. Semenov, K.F. Renk: Opt. Lett. **17**, 502 (1992)
24. P.T. Lang, W. Schatz, K.F. Renk: Opt. Comm. **84**, 29 (1991)
25. T.A. DeTemple: in *Reviews of infrared and millimeter waves*, Vol.2, K.J. Button ed. (New York: Plenum Press 1983) p.337
26. B.G. Danly, S.G. Evangelides, R.J. Temkin, B. Lax: in *Infrared and millimeter waves*, Vol.12, K.J. Button ed. (New York: Academic Press 1984) p.195
27. Y. Nishi, A. Murai: Int. J. Infrared Millim. Waves **11**, 309 (1990)